Contribution of Pumped Storage Units to Mixed Islanded Power Network Stability

C. Nicolet	A. Béguin	B. Kawkabani	C. Landry	F. Avellan
Power Vision Engineering sàrl 1 ch. Champs-Courbes 1024 Ecublens Switzerland	Power Vision Engineering sàrl 1 ch. Champs-Courbes 1024 Ecublens Switzerland	EPFL Electrical Machinery Group 1015 Lausanne Switzerland	EPFL Laboratory for Hydraulic Machines 1015 Lausanne Switzerland	EPFL Laboratory for Hydraulic Machines 1015 Lausanne Switzerland

Abstract

This paper presents the modeling, simulation and analysis of the dynamic behavior of a mixed islanded power network of 1'850 MW comprising 1'300 MW of coal fired thermal power plant, 200 MW of wind power, 100 MW of photovoltaic installed capacity and a 250 MW pumped storage power plant. First, the modeling of each power plant is fully described. The model of the thermal power plant includes a high-pressure steam turbine and 2 low-pressure steam turbines, the rotating inertias, and a 1'400 MVA turbo-generator with power controller and a voltage regulator. The 200 MW wind farm is modeled using an aggregated model of 100 wind turbines of 2 MW unit power. The wind farm model comprises a stochastic model of wind evolution with wind gust, a power coefficient based model of wind turbine with a-priori controller and a synchronous generator with voltage regulator. The 100 MW photovoltaic power plant is also modeled using an aggregated model. This model includes variable lightening source, a PV voltage source characteristic curve function of the light intensity and PV system current, an a-priori control system for maximum power tracking and a two level voltage source inverter. Finally, the 250 MW pumped storage power plant model comprises the upstream reservoir, a 2'000 m gallery, a surge tank, the 900 m long penstock feeding a fixed speed unit pump-turbine connected to the downstream tank through a 250 m long tailrace water tunnel. The 4 power generation plants are connected to a passive consumer load via a 500 KV electrical line network. Then, the capability of the pumped storage plant to contribute to the islanded power network stability is investigated through the time domain simulation of the dynamic behavior of the entire mixed power network using the simulation software SIMSEN. The stability of the power network is analyzed in terms of frequency and voltage deviations induced by PV output power fluctuations. Three scenarios are presented, each with a different control strategy for the hydropower.

1. Introduction

Increasing the penetration of renewable energy sources such as wind and photovoltaic power in small power networks, as shown in Figure 1, is a challenging task as far as the power network stability is concerned. Indeed, as solar and wind energy are highly volatile sources, islanded power networks featuring high level of wind or solar power penetration are subjected to undesired perturbations affecting the power network stability [24]. Nevertheless, pumped storage plants can significantly improve the stability of mixed islanded power network due to their production flexibility**.** However, the planning, design and optimization of new pumped storage units developed to compensate renewable energy volatility requires detailed analysis of the power network stability. In this context, advanced simulation models of each power plant are necessary to investigate the power network dynamic behavior and address the power network stability for various configurations and scenarios.

The dynamic of the pumped storage plants can be improved using either a variable speed layout or compound ternary machine type unit. The high dynamic performances of such pumped storage plants are of highest interest for improving stability of mixed islanded power network. The compound ternary machine type units, with turbine, generator, fluid coupling clutch and pump, offer also numbers of operation advantages despite a higher investment cost compared to variable speed pump-turbine. The operation advantages of the compound ternary machine type units are the following [4], [14]: (*i)* increased efficiency in pump and turbine modes, (*ii)* high operational flexibility due to rapid change of operation mode from pump to turbine and vice-versa, (*iii)* easy and short time start-up in pump mode, (*iv*) adjustable pump power in hydraulic short-circuit operation, (*v*) efficient condenser modes. The variable speed pump-turbine layout features nevertheless faster response, thanks to the power electronics, see [10], [15].

The wind power delivered to the grid is dependent on the wind velocity and its stochastic variation. The wind speed is composed of a mean value and wind gusts. The power variations due to wind gusts are damped by the rotating inertia of the rotor. However, the variation of the mean value will perturb the grid. Nowadays, weather

forecast services can predict precisely enough such variations so that the grid operator can schedule it. Despite the prediction of wind velocity, pumped storage plants are still needed to improve the grid stability. The references [14] and [15] present a study of the contribution of hydropower plant to islanded grid stability when wind power is connected.

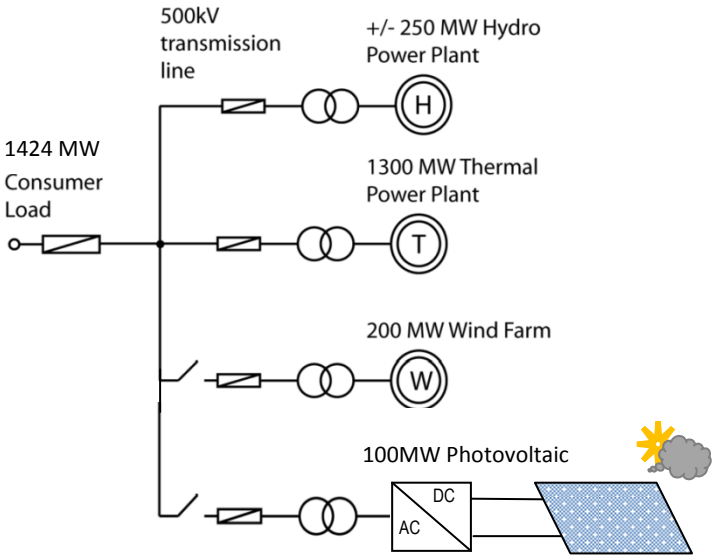

Figure 1 Mixed islanded power network.

In a similar way, Photovoltaic (PV) power plants are also subject to uneven generation due to the sun global irradiation variations. There is the normal daily irradiation variation due to the Earth rotation. This is a slow variation that can easily be taken into account by grid operator. Besides, there is an irradiation variation due to clouds that can shield the PV panels, cutting them from the direct beam of the sun. However, there is still the diffusion irradiation and PV panels can generate power but at a reduced level. Figure 2 shows a representative variation of sun global irradiation during the day, for a clear day and for a cloudy day. The spikes are due to clouds passage. It can be observed that, for a clear day, such temporary clouds represent a loss of 50% of the irradiation. For cloudy day, sudden cloud dissipation can represent an increase by five time of the irradiation.

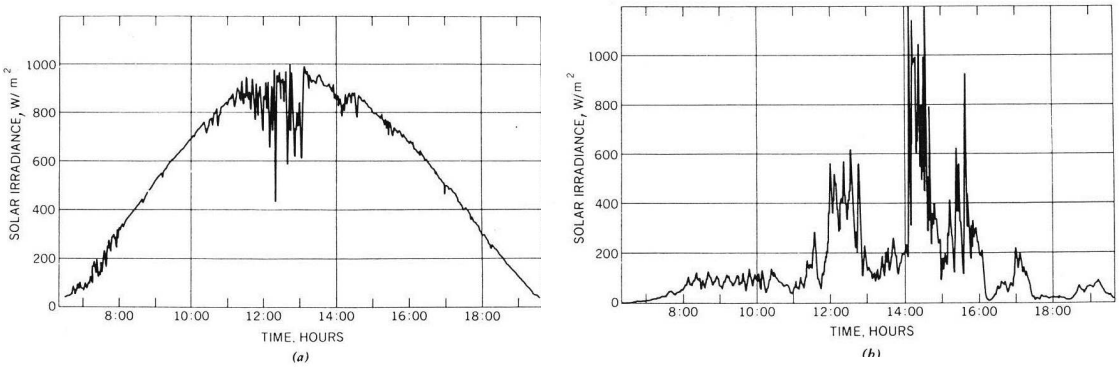

Figure 2 Typical sun's global irradiation for a clear *(a)* and a cloudy *(b)* day
(source: "Solar Energy Systems Design" by W.B.Stine and R.W.Harrigan [22]).

The maximum theoretical irradiation is about 1'360 W/m^2 and is the irradiation of the beam hitting the earth's atmosphere. In a first approximation, the maximum output power of the PV panels is proportional to the irradiation. The time constant of the cloud passage phenomenon is not clearly defined but it can be reasonably assumed that the sun direct beam can be covered in a few seconds. The power variations are hence even faster than they are for the wind. Moreover, the PV cells do not contain any energy storage device. If there are any, they are placed on purpose in the power conversion device. So as for the wind power, solar power variations must be analyzed to assess their impact on the grid stability. The power range of PV power plants is increasing and reaches the 100 MW nowadays and will reach the 500 MW in 2015 [26], most of the latter being built in

deserts. The degree penetration of solar power plant into the large grids is nowadays small. However, it is much more different for islanded network, indeed where solar power is inclined to be used.

This paper presents the modeling, numerical simulations and analysis of the stability of a mixed islanded power network of 1'850 MW capacity, depicted in Figure 1, comprising 1'300 MW of classical thermal power plant, 200 MW of wind power, 100 MW of solar power and 250 MW of hydropower. Apart from the hydro power, the ratio of renewable power to the total power is 11% and 5% for resp. the wind and the solar plants. The four power plants are connected to a passive consumer load via a 500 KV electrical line network as presented in Figure 1. The hydraulic power plant features a compound ternary machine type unit with fixed speed synchronous motor-generator.

First, the modeling of each power plant is described with a particular focus on the solar power plant. Then, the capability of the pumped storage plant to stabilize the islanded power network is investigated through the time domain simulation of the dynamic behavior of the entire mixed power network using the software SIMSEN. The reference case is a steady state of the power network with constant wind and solar power, at their rated level and with a pumped storage plant pumping the excess of power. Besides the reference case, three different scenarios are considered: *i)* fluctuations of sun irradiation without contribution of hydropower plant in frequency control, *ii)* fluctuations of solar power with hydropower plant participating in the frequency control, *iii)* fluctuations of solar power with hydropower plant participating in the frequency compensations with power measurement. Safe and stable operation for the 3 above mentioned scenarios are presented. Then the comparison of case *i)*, *ii)* and *iii)* enables to emphasize the benefits of the hydro power plant contribution to grid stability and advantage of advanced frequency control method.

2. Modeling of the Hydraulic Machinery and Systems

By assuming uniform pressure and velocity distributions in the pipe cross section and neglecting the convective terms, the one-dimensional momentum and continuity balances for an elementary pipe filled with water of length *dx*, cross section *A* and wave speed *a*, see Figure 3, yields to the following set of hyperbolic partial differential equations [25]:

$$\begin{cases} \dfrac{\partial h}{\partial t} + \dfrac{a^2}{gA} \cdot \dfrac{\partial Q}{\partial x} = 0 \\ \dfrac{\partial h}{\partial x} + \dfrac{1}{gA} \cdot \dfrac{\partial Q}{\partial t} + \dfrac{\lambda |Q|}{2gDA^2} \cdot Q = 0 \end{cases} \quad (1)$$

The system (1) is solved using the Finite Difference Method with a 1st order center scheme discretization in space and a scheme of Lax for the discharge variable. This approach leads to a system of ordinary differential equations that can be represented as a T-shaped equivalent scheme [9], [17], [21] as presented in Figure 4. The RLC parameters of this equivalent scheme are given by:

$$R = \frac{\lambda \cdot \left|\overline{Q}\right| \cdot dx}{2 \cdot g \cdot D \cdot A^2} \quad L = \frac{dx}{g \cdot A} \quad C = \frac{g \cdot A \cdot dx}{a^2} \quad (2)$$

Where λ is the local energy loss coefficient. The hydraulic resistance *R*, the hydraulic inductance *L*, and the hydraulic capacitance *C* correspond respectively to energy losses, inertia and storage effects.

The model of a pipe of length *L* is made of a series of n_b elements based on the equivalent scheme of Figure 4. The system of equations relative to this model is set-up using Kirchoff laws. The model of the pipe, as well as the model of valve, surge tank, Francis turbine, etc., is implemented in the EPFL software SIMSEN, developed for the simulation of the dynamic behavior of hydroelectric power plants, [12], [18]. The time domain integration of the full system is achieved in SIMSEN by a Runge-Kutta 4th order procedure.

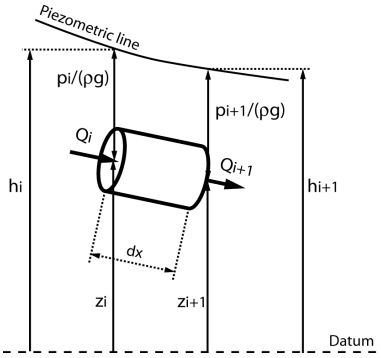

Figure 3 Elementary hydraulic pipe of length *dx*.

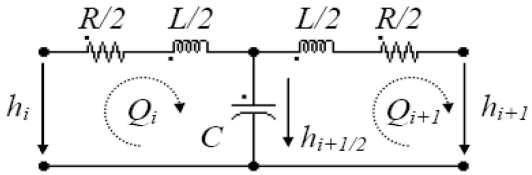

Figure 4 Equivalent circuit of an elementary pipe of length *dx*.

The modeling approach based on equivalent schemes of hydraulic components is extended to all the standard hydraulic components such as valve, surge tanks, air vessels, cavitation development, Francis pump-turbines, Pelton turbines, Kaplan turbines, pump, etc., see [12].

3. Hydraulic Power Plant Model

The layout of the hydraulic power plant is presented in Figure 5. The power plant is made of an upstream reservoir, a 1'950 m long gallery, a 885 m long penstock connected to a hydroelectric power house of +/- 250 MW with a compound ternary machine type arrangement with fixed speed synchronous generator of 280 MVA, connected to the downstream reservoir by a tailrace water tunnel of 250 m long. Table 1 gives the main characteristics of the pumped-storage power plant. The hydraulic machines are modeled using their 4 quadrants hydraulic characteristics. The model of the piping system accounts for detailed water-hammer and mass oscillation phenomena, [12].

Table 1 Pumped-storage power plant characteristics.

Pump / Turbine	**Generator**
P_R = 250 MW	Rated apparent power: 280 MVA
N_R = 500 min^{-1}	Rated phase to phase voltage: 17.5kV
Q_R = 55 m^3/s	Frequency: 50 Hz
H_R = 510 m	Number of pairs of poles: 6
ν = 0.22	Stator windings: Y
$J_{pump\text{-}turbine}$=1.05 x 10^5 kgm^2	J_{rotor}=8.1 x $10^5 kgm^2$

The model of the compound ternary units considered in this paper is presented in Figure 5. This model is composed of a Francis turbine of 250 MW, the synchronous generator of 280 MVA, a pump of 250 MW and a clutch between the generator and the pump. The clutch characteristic is taken from [2]. The turbine is equipped with a PID turbine speed governor and the generator is controlled by an ABB Unitrol voltage regulator. The model of the generator is based on 1 equivalent rotor circuit in the direct-axis and 1 equivalent rotor circuit in the quadrature-axis allowing taking into account a sub-transient behavior, see [5].

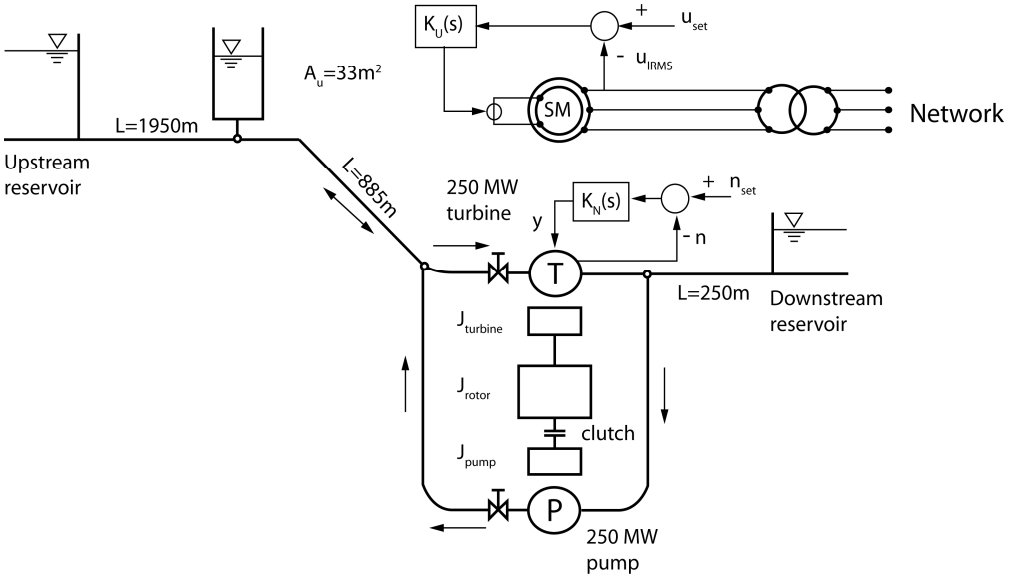

Figure 5 Pumped storage power plant model with fixed speed and 3 machine-type arrangements.

4. Thermal Power Plant Model

The model of the 1.3 GW thermal power plant is based on steam flux and takes into account a constant pressure steam vessel, a regulating valve, a high pressure steam turbine, a steam transit through a re-heater and two low pressure steam turbines as presented in Figure 6. The model is based on valve and torque characteristics deduced from [3], on first order transfer functions for the turbine dynamics with τ_{HP} , τ_{LP} time constants, a re-heater modeled by a time delay *b*, and on a proportional regulator of constant *Kp*. The shaft line comprises 4 rotating inertias connected by 3 shafts with given stiffness and damping. And finally a turbo generator with 2 pairs of poles is also included in the model with the ABB Unitrol voltage regulator. The model of the generator is based on 2 equivalent rotor circuits in the direct-axis and 1 equivalent rotor circuit in the quadrature-axis considering saturation, leakage and damping effects of windings, allowing taking into account a sub-sub-transient behavior, see [5]. The parameters of the model are given in Table 2 and details of the model can be found in [13].

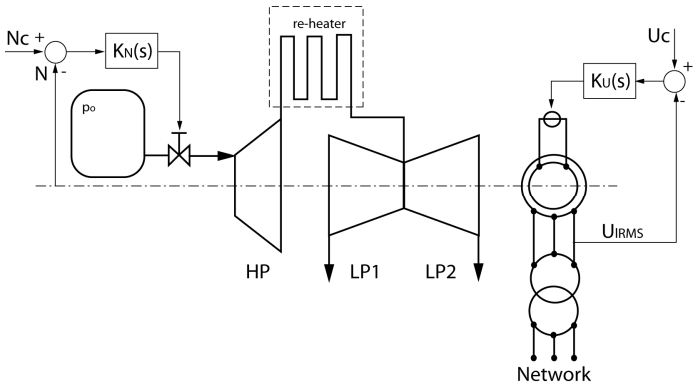

Figure 6 Thermal power plant model.

Table 2 Thermal power plant characteristics.

Steam turbines model	Mechanical masses inertias	Mechanical shaft stiffness and damping	Generator
τ_{HP} = 0.5 s τ_{LP} = 12 s *b* = 4 s *Kp* = 25	J_{HP} = 1.867 10^4kgm^2 J_{LP1} = 1.907 10^5kgm^2 J_{LP2} = 2.136 10^5 kgm^2 J_{GEN} = 5.223*10^4 kgm^2	K_1 = 3.614 10^8 Nm/rd K_2 = 8.206 10^8 Nm/rd K_3 = 4.116 10^8 Nm/rd μ_1 = 6.719 10^3 Nms/rd μ_2 = 7.06 10^3 Nms/rd μ_3 = 7.06 10^3 Nms/rd	Rated apparent power: 1400 MVA Rated phase to phase voltage: 28.5 kV Frequency: 50 Hz Number of pairs of poles: 2 Stator windings: Y

5. Wind Farm Model

5.1. Wind Turbine Model

The model of a 2 MW wind turbine is presented in Figure 7. It includes a model of the turbulent wind, the turbine with adjustable blade pitch angle θ and inertia $J_{turbine}$, the shaft stiffness k_{shaft}, the gear box, the synchronous generator of 2 MVA with voltage regulator and the transformer. The characteristics of the wind turbine model are given in Table 3. The model of the generator is based on 1 equivalent rotor circuit in the direct-axis and 1 equivalent rotor circuit in the quadrature-axis allowing taking into account a sub-transient behavior, see [5].

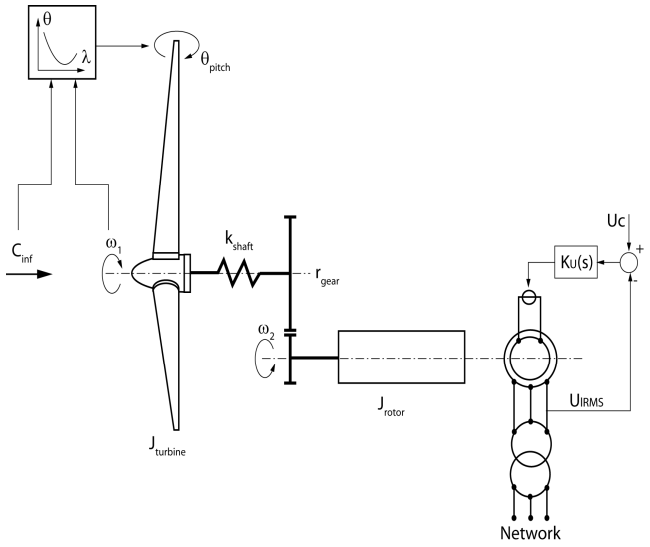

Figure 7 Wind turbine model.

Table 3 Wind turbine characteristics.

Operating datas	Wind turbine	Mechanical system	Generator
Cut-in wind velocity: 3.5 m/s Cut-out wind velocity: 20 m/s Rated wind velocity: 13 m/s	Number of blades: 3 Diameter: D = 75 m Rotational Speed: n_1 = 24.75 min^{-1}	r_{gear}= 3.032 k_{shaft} = 2.2 10^8 Nm/rd $J_{turbine}$= 3.15 10^6 kgm^2 J_{rotor}= 6.48 10^4 kgm^2	Rated apparent power: 2 MVA Rated phase to phase voltage: 400 V Frequency: 50 Hz Number of pairs of poles: 40 Stator windings: Y

The turbulent wind model is composed of a wind mean value and a wind gust, as suggested by Slootweg *et al.* [19]. The turbulent gust is modeled by a Pseudo-Random-Binary-Sequence, PRBS, obtained by a shift register method, see [7]. The mechanical power transmitted by the fluid to the wind turbine can be expressed as:

$$P = \frac{1}{2}\rho \cdot Aref \cdot Cp \cdot C_{\inf}^3 \quad (3)$$

Where A_{ref} is the swept area and C_p is the power coefficient and ρ is the air density. Heier [8] provides an empiric approximation of the wind turbine power coefficient C_p as function of the tip speed ratio λ is defined as:

$$\lambda = \frac{U_t}{C_{\inf}} = \frac{D_{ref} \cdot \omega_1}{2 \cdot C_{\inf}} \quad (4)$$

Where U_t is the blade tip velocity, C_{inf} is the wind velocity and ω_1 is the wind turbine rotating pulsation. Figure 8 left presents the power coefficient C_p of a wind turbine as function of the tip speed ratio λ and of the blade pitch angle θ obtained according to [8].

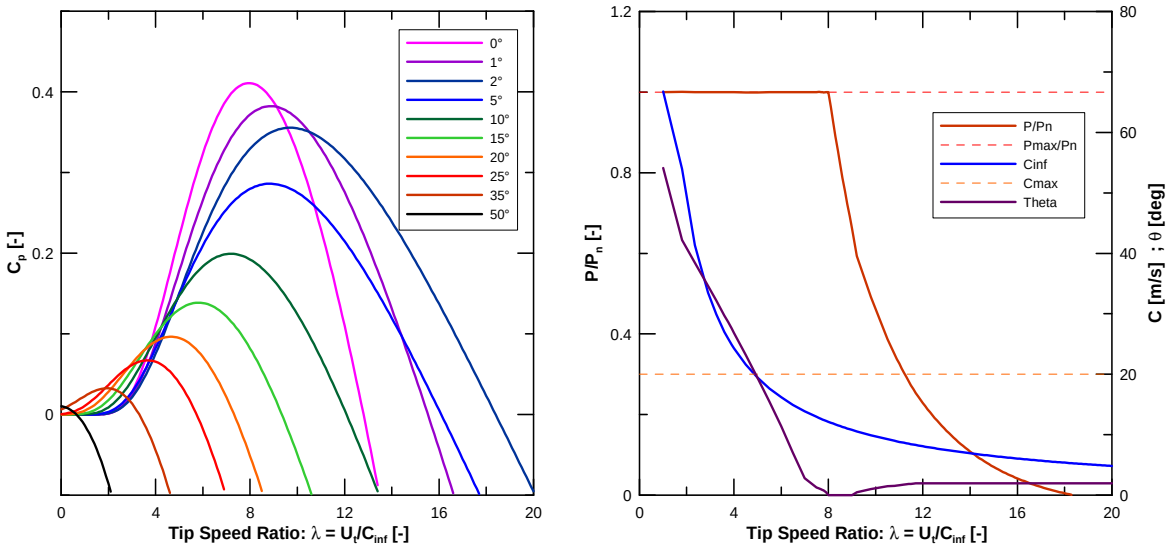

Figure 8 Wind turbine characteristic according to equation (4) (left) and wind turbine power, pitch angle and wind velocity and related limits as function of the tip speed ratio (right).

Then, the wind turbine output power is calculated from the characteristics given in Figure 8 left, as function of the tip speed ratio as presented in Figure 8 right, see also [20]. The blade pitch angle given as function of the tip speed ratio is also represented in Figure 8 right. For tip speed ratio above 8, the pitch angle is selected to provide the highest power coefficient while below 8 it is selected to generate the 2 MW output power limit. The blade pitch angle θ is driven by a look-up table as function of the tip speed ratio λ as represented in Figure 8 right.

5.2. Aggregated Wind Farm model

For power grid stability purposes, it is possible to use an aggregated wind farm model, consisting of one wind turbine equivalent to *n* single wind turbines as presented in Figure 9, see [1]. Then according to the energy conservation and in order to keep the same torsional mode eigenfrequency, the active power P_n, rotating inertias *J*, the shaft stiffness k_{shaft} and the swept area A_{ref} are multiplied by the number of wind turbines *n*. The parameters of the synchronous generator being given in per unit, they are kept constant. For the present study, only one equivalent machine can be used as no electrical faults are considered [1].

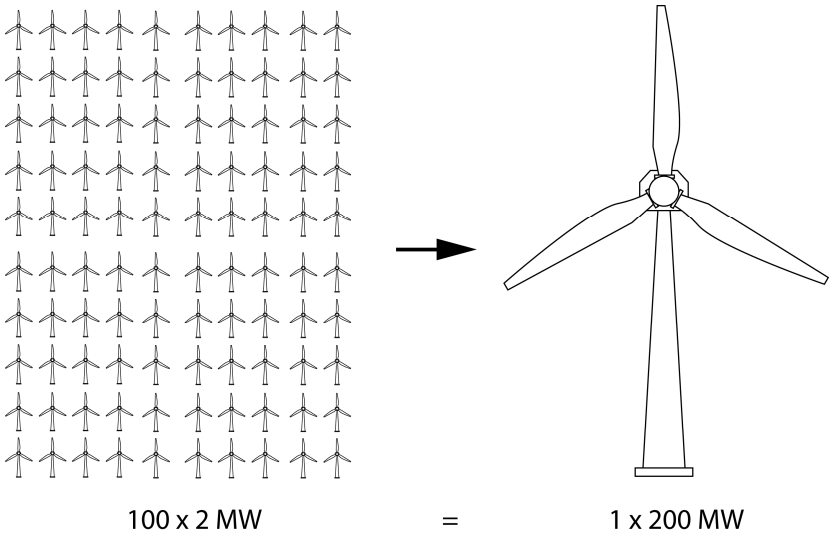

Figure 9 Wind turbine farm of 100 x 2 MW modeled as an equivalent wind turbine of 200 MW.

6. Photovoltaic Power Plant

The solar power plant has two main components, the photovoltaic (PV) cells arrays and the power converter to inject AC power into the grid from the continuous current (DC) PV arrays.

6.1. Photovoltaic panels

The PV arrays are built from PV panels and panels are built from PV cells, as shown in Figure 11. A PV panel is an array of series and parallel connections of PV cells to reach desired voltage and current levels. The typical static voltage-current characteristic of a PV panel is given in Figure 10. As a PV cell, a PV panel behaves as a current source when short circuited and as a voltage source in open circuit. Figure 10 shows a typical PV panel with a rated maximum power of 260 W with V_{oc} of 60 V and I_{sh} of 5.5 A, for a rated irradiation of 1000 W/m^2. The static characteristic varies with the solar global irradiation and the cell temperature. Mainly, the short circuit current (I_{sh}) varies with the irradiation while the open circuit voltage (V_{oc}) varies with the temperature. However, the shape of the characteristic remains identical. The power delivered by the panel has an obvious maximum point, as shown in Figure 10, corresponding to an optimal cells operating voltage U_{PVmax} and current I_{PVmax}. In general, when harvesting solar power, the control system attempts to stay on this maximum power point by permanently adapting the impedance seen by the PV panels. This is known as Maximum Power Point Tracking (MPPT) control.

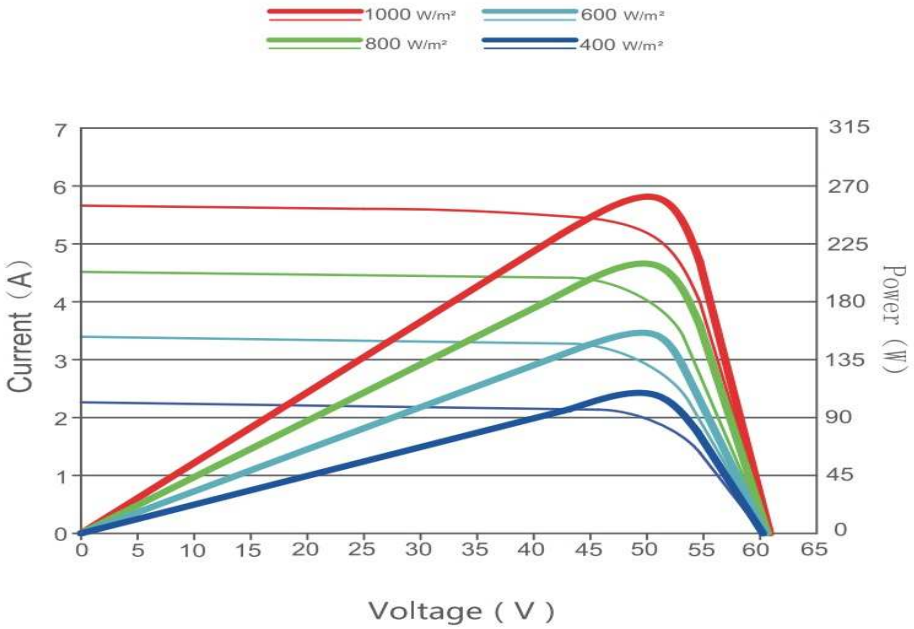

Figure 10 Voltage-current static characteristics of a PV panel, deduced from [27].

6.2. Aggregated model of PV power plant: the PV arrays

To build a solar power plant of several MW or several hundreds of MW, the PV panels are arranged in series and parallel to build PV blocks of a given power. Nowadays, the maximum working voltage (common mode voltage) of a PV panel is between 600 V_{dc} and 800 V_{dc}, depending on the standards used. This is mainly due to the limitation of insulation between PV cells and the ground. Also, the series connection of PV cells imposes constraints on voltage equilibrium among all series connected cells to ensure that individual cell voltage does not go beyond the maximum allowed. The maximum admissible common voltage of a PV panel imposes the maximum nominal voltage of one PV block, which is at most 800 V_{dc}. Nowadays typical nominal power of a PV block is 1 MW in the biggest solar power plants. This is feasible since power semiconductors, which are used to build the power converter, are easily available with similar voltage and current ratings. To reach the total power of the solar plant, several of those blocks are operating in parallel. They each have their own power converter. For a 100 MW solar plant, this means that there are 100 of those blocks. Despites the multiplication of blocks and hence of components of the power plant, this architecture offers modularity, efficiency by paralleling currents, and reliability. In case of a converter fault, only the faulty blocks must be disconnected.

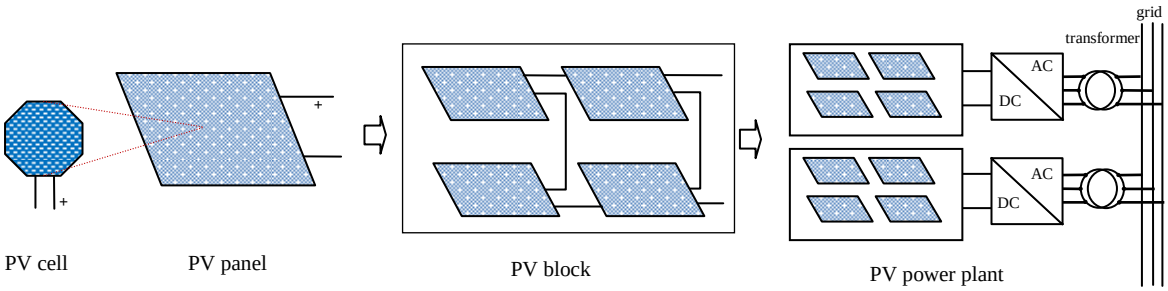

Figure 11 From PV cell to PV power plant.

For the present study, all the series and parallel connections are equivalent to a simple scaling of the PV panel UI-characteristic, which is only an approximation since impedance of connections are neglected. Moreover, the paralleling of the PV block is modeled as an equivalent unique block because it is not of interest to model each PV block here. The equivalent PV block must have the same nominal impedance than the individual PV block ("Thevenin" equivalent source). This means that the UI characteristic of the PV block is scaled by $\sqrt{n}$ for U and I, where n is the number of PV blocks, to obtain the characteristic of the equivalent, or aggregated, PV source.

In the simulation software SIMSEN, the equivalent PV source is modeled as a current driven voltage source, as shown in Figure 12. The voltage of the source is a function of its current. The analytical law of the characteristics is implemented. Its parameters depend on the sun's irradiation, but are valid for a constant temperature only (25°C).

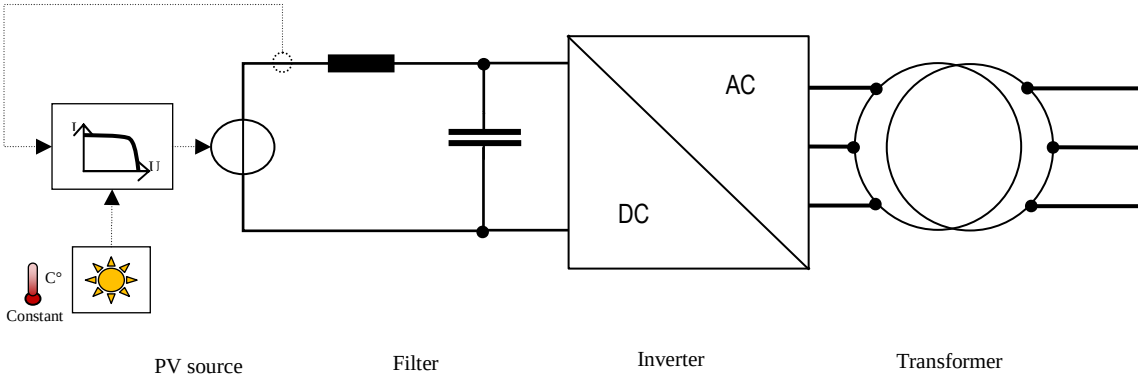

Figure 12 PV plant model implemented in SIMSEN Software.

6.3. Power converter

The power converter must interface the DC source, the PV arrays, to an AC source, the power network. This is usually called an inverter. In power electronics, there are many variants to build an inverter, depending on the switching frequency, the commutation mode (Pulse Width Modulation (PWM) or square wave) and circuit execution [11]. It is also possible to include the voltage elevation transformer in order to shift its frequency to medium frequency and hence shrink the transformer's size. The semiconductor commutation circuit can also be optimized to minimize the commutation losses. For the scope of this paper, a simple three-phase two levels inverter running in PWM mode is used. PWM mode is preferred here to square wave in order to simplify the filter required at the output of the converter to filter out the current harmonic injected into the network. However, the efficiency might be better in square wave mode. The converter output is connected to a line frequency step-up transformer that adapts to the grid high voltage. Between the PV source and the inverter, there is a low pass filter which consists in an inductor and a capacitor. This is to filter out the high frequency component of the current as the PV source is a DC source which is not made to support high frequency current ripples. Consequences of current ripple on the performance on PV source could be faster aging and reduced efficiency.
In the SIMSEN simulation software, the inverter is modeled at the transistor level, see Figure 13, which means that the real PWM output voltage is computed.

6.4. Control of the PV plant

For PV power plant, the power delivered to the grid is controlled via the inverter and can have a very fast response compared to other sources in the network that involves rotating inertias. The power could go from 0 to 1 per unit or reverse in a few tens of ms. The dynamic depends here on the PV source and the bandwidth of the DC and AC side filters. Also, power variation limitations could come from the grid code. The dynamic of the converter is anyway faster than most of the phenomena which it has to regulate (sun light variation, grid transient phenomena). The power converter has also the ability to control the amount of active power *P* and reactive power *Q* that are injected. The PV plant could hence also offer voltage support services to the network by injecting reactive current. A study of the *P* and *Q* capability of a PV power plant can be found in [6]. In this paper, the solar plant is always operated with a unity power factor hence delivering only active power.

In a real PV plant a part of the control is the MPPT which always exploit the PV source to its maximum power capacity, depending on the solar irradiation and temperature. The MPPT algorithm looks for the optimal operating impedance of the PV source in a "trial and error" manner because this point cannot be known in advance and is subject to change with sun's irradiation change, temperature and aging. The operating point is permanently slightly perturbed around a set value which is adjusted in consequence depending on the result of the perturbation. The output of the MPPT is the set value for the control of the converter. The inverter hence has a control for example of the input DC voltage which itself is controlled by an inner current controller. In this paper, for simplicity purposes, an a-priori MPPT is considered. It means that the optimal impedance is known from the PV characteristic and hence the power converter is set to reach this operating point, with a given delay that accounts for the delay in a real MPPT.

7. Mixed Islanded Power Network Model

Figure 13 presents the full SIMSEN model of the mixed islanded power network of Figure 1 based on the hydraulic, thermal wind and solar power plant models described above. The model also includes the 500 kV transmission lines and the passive consumer load.

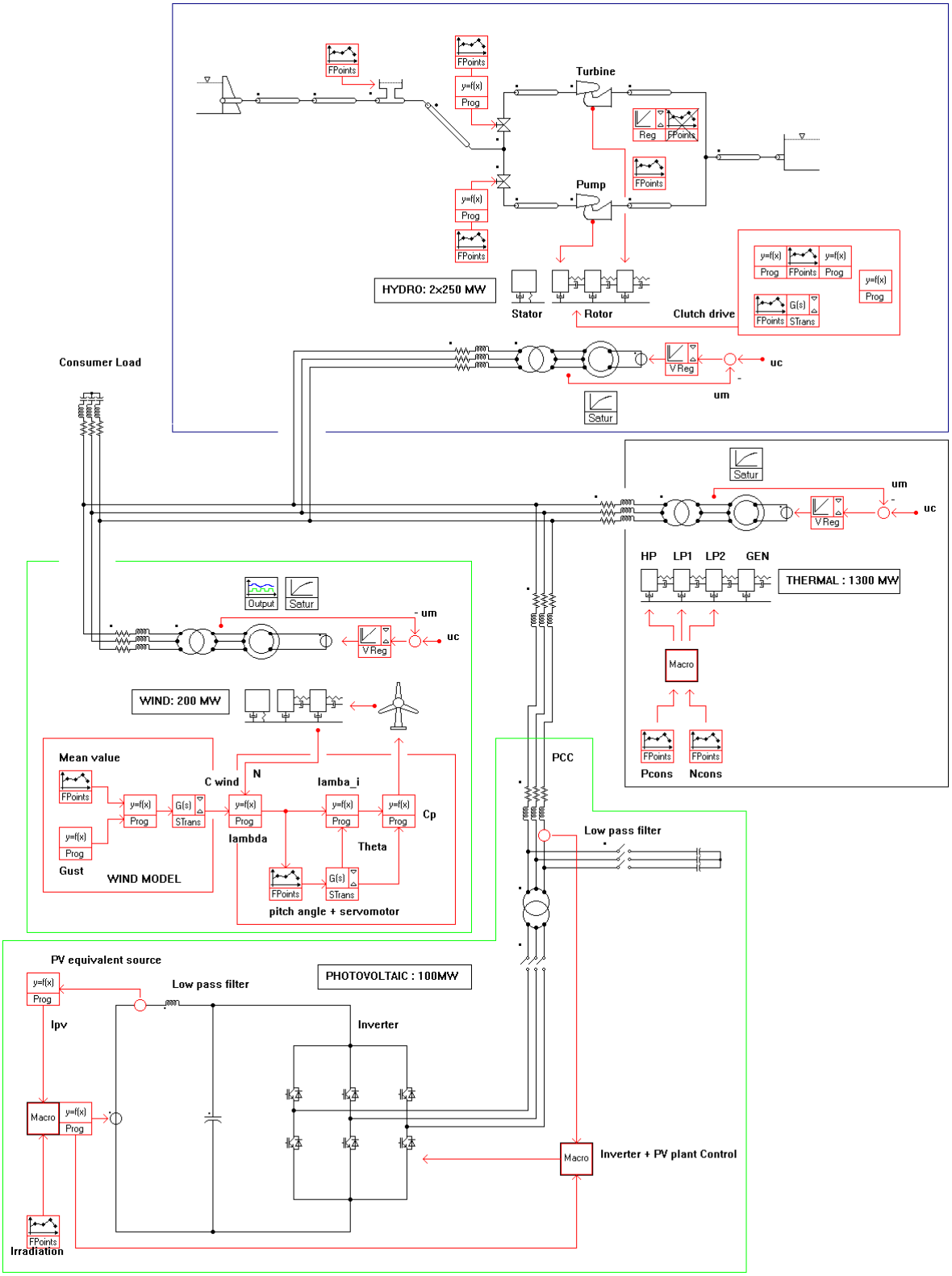

Figure 13 Mixed Islanded Power Network SIMSEN model.

8. Transient Behavior of Mixed Islanded Power Network

Besides the reference case, three different cases study are considered for the analysis of the dynamic behavior of the mixed islanded power network. All three cases simulate a sudden decrease of solar irradiation representing a cloud passage. Then, for each of the three cases, a different control of the pumped storage plant is used:

i) no frequency compensation;
ii) the pumped storage power plant provides secondary control based only on frequency deviation measurement with a PID turbine governor;
iii) the pumped storage power plant provides secondary control based on frequency deviation and power unbalance detection with PID turbine governor.

The scenarios and simulation results related to the three case studies stated above are described in the following subchapters.

8.1. Reference case

The reference case consists in a situation with a constant renewable power input. The sun global irradiation is kept at 1000 W/m^2, the rated value. The solar power plant injects its nominal power into the grid. There are only wind gusts as perturbations. The initial conditions of the power flow of the islanded power network are summarized in Table 4. The thermal, wind and solar power plants are in generation operating conditions, close to rated output power while the consumer load is consuming 1'400MW and the pumped storage plant is pumping about 168MW because of the excess of power production and is operated in hydraulic short-circuit between the pump and the turbine. The difference between the production and consumption corresponds to the energy losses in transmission lines and transformers.

Table 4 Initial power flow.

Element	Active power P [MW]	Power flow
Hydropower Plant	168.1	Consumption
Thermal Power Plant	-1288	Production
Wind Farm	-185.6	Production
PV power plant (at PCC)	-97.8	Production
Consumer Load	1400	Consumption

Figure 14 shows the waveforms at the output of the inverter of the PV plant. The inverter switching frequency is about 4 kHz. The ripples in the output current are filtered out by a low pass filter (shown in Figure 13) to comply with grid codes. Filtered voltage and current at the point of common connection (PCC) of the PV power plant are shown in Figure 15. Figure 14 shows also the voltage and current of the PV source, which are constant and with negligible ripples. The inverter controls the current injected into the grid, at the high voltage side of the step-up transformer. This current is set so that the PV plant injects only active power, as shown in Figure 16. In this figure, the PV reactive power is represented by the light blue curve and is obviously nil.

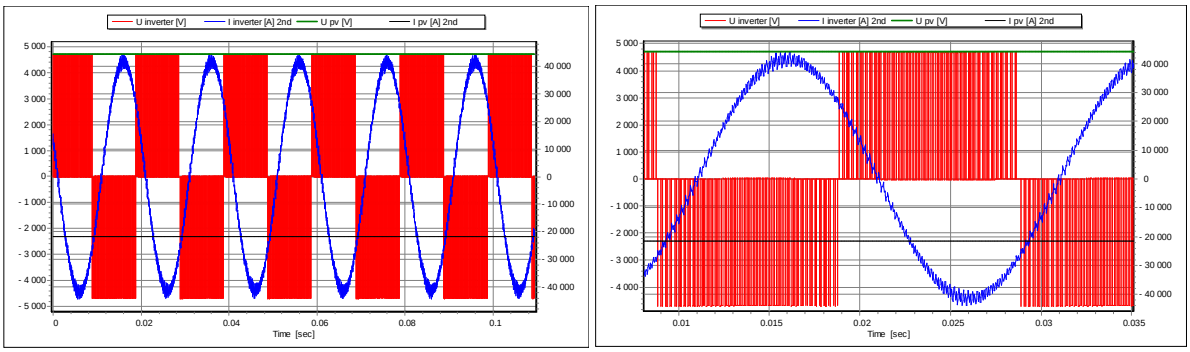

Figure 14 Voltage and current of PV source and at output of inverter.

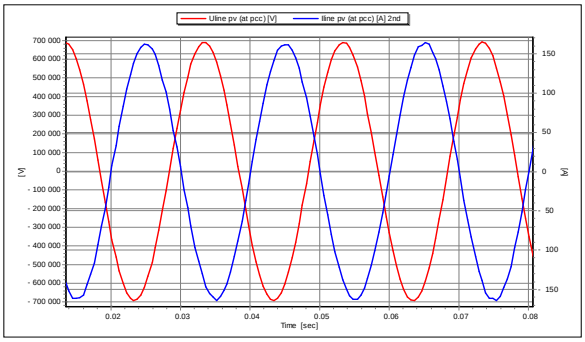

Figure 15 line voltage and line current of PV plant at PCC.

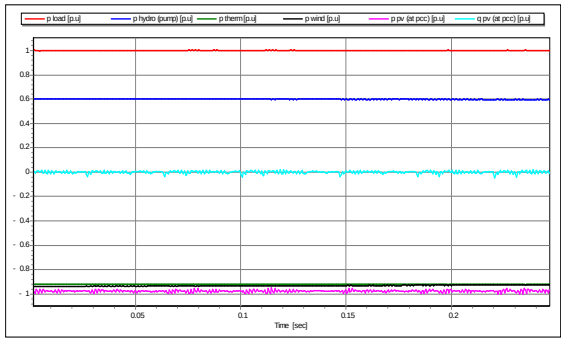

Figure 16 Active and reactive power levels for each plant in the mixed islanded power network.

8.2. Sudden decrease of the sun's irradiation without frequency compensation (case *i)*

The initial conditions of the power flow in the islanded power network are identical to the reference case (Table 4). The sun's irradiation falls from 1000W/m^2 to 500W/m^2 in about five seconds, representing a sudden cloud passage, as represented in Figure 17. The decrease of irradiation changes the static characteristic of the PV source. This phenomenon can be observed in Figure 17 when looking the voltage of the PV source which decreases while irradiation and PV current decrease. This means that the power delivered by the PV source decreases. The control of the PV plant detects this drop in power and permanently adapts the set value of the inverter control to extract the maximum power possible of the PV source, as in Figure 18, which shows the current injected into the grid by the PV power plant. This power decreases from its nominal value to 0.45 p.u in about 5 seconds, as represented in Figure 19. It can also be noted that the reactive power is kept nil all the time by the PV plant controller, except during the transient response where a very small amount of reactive power is injected. A more advanced, and existing, current controller could solve easily this problem, known as "coupling" of *P* and *Q* components.

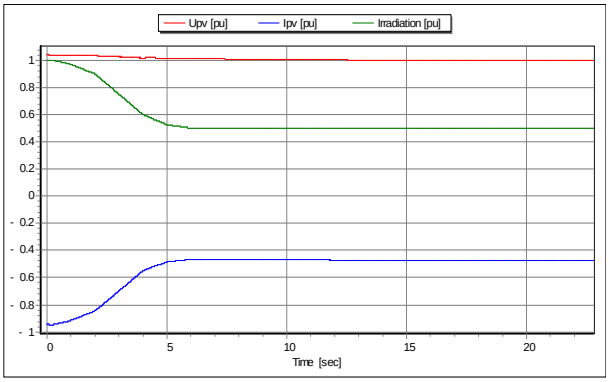

Figure 17 Decrease of irradiation and PV voltage and current.

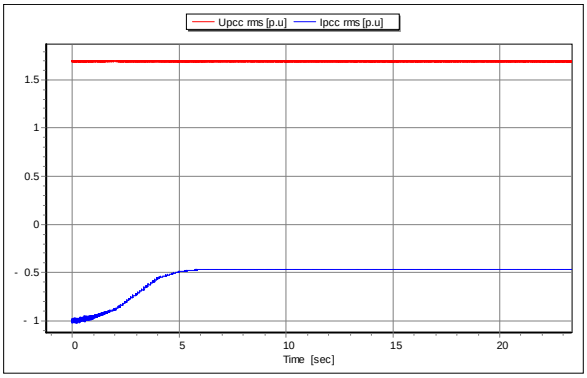

Figure 18 Voltage and current (rms) at the PCC of the PV plant.

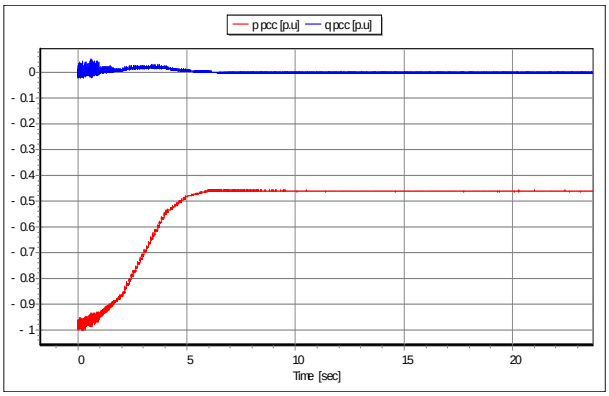

Figure 19 Active (P) and reactive (Q) power at PCC of the PV plant.

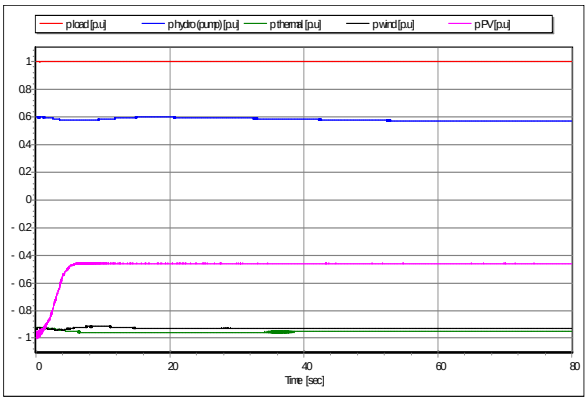

Figure 20 Active power for all 4 power plants.

As it can be observed in Figure 20, the power consumption is in excess on the network because of the sudden decrease of solar power. Consequently, the other plants of the network must increase their production to reach a new power balance. Because of the under production, the frequency of the network decreases until the primary control stabilizes the production and consumption balance. This primary control is essentially done in the thermal power plant. In Figure 20, only the power production of the thermal plant has been changed to compensate for the over consumption. This primary control takes about 10s to stabilize the frequency, which is stabilized at about 0.998 p.u, i.e. 49.9 Hz. In this scenario, the hydropower plant, in pump mode, consumes a constant power, indeed, as shown in Figure 21 and Figure 22, the guide vane opening of the turbine remains constant,. There is no plant that provides secondary control with power setpoint change, and therefore the frequency deviate from the nominal value after the perturbation. Depending on the grid code specification, this situation could be acceptable or not, or only acceptable for a limited duration.

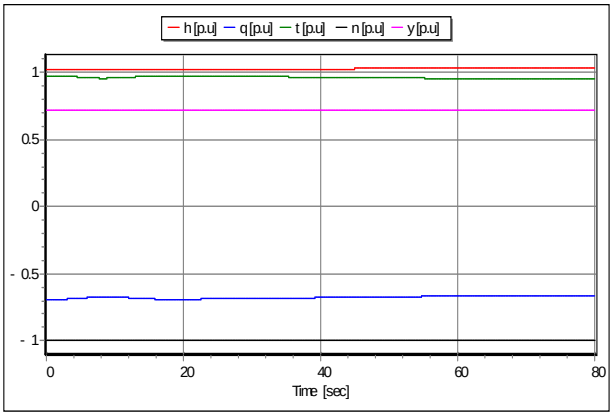

Figure 21 Transient behaviour of the pump during the decrease of irradiation.

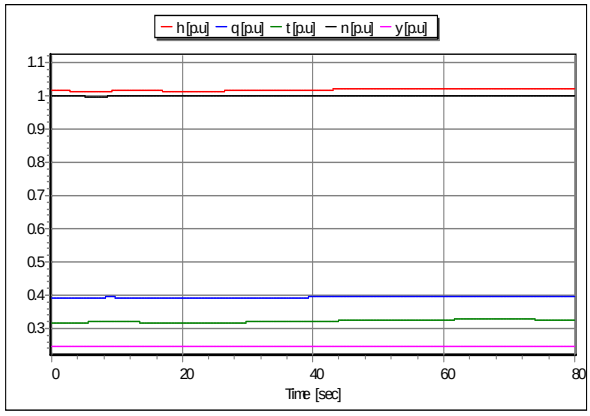

Figure 22 Transient behaviour of the turbine during the decrease of irradiation.

8.3. Sudden decrease of the sun's irradiation with secondary control based on frequency deviation (case *ii)*

The initial conditions of the power flow in the islanded power network are identical to the reference case, see Table 4. The same scenario as in section 8.2 is presented here, see Figure 23, except that the control of the pumped storage power plant includes a secondary control with frequency compensation carried out by the turbine governor while the pump remains in normal operation.

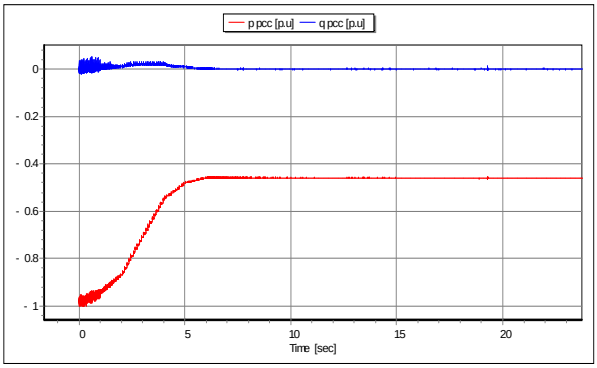

Figure 23 Active (P) and reactive (Q) power at PCC of the PV plant.

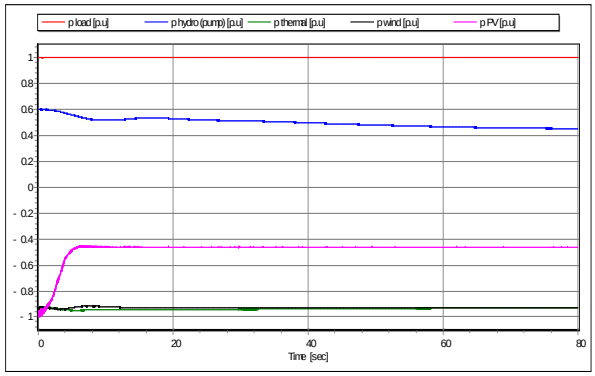

Figure 24 Active power for all 4 power plants.

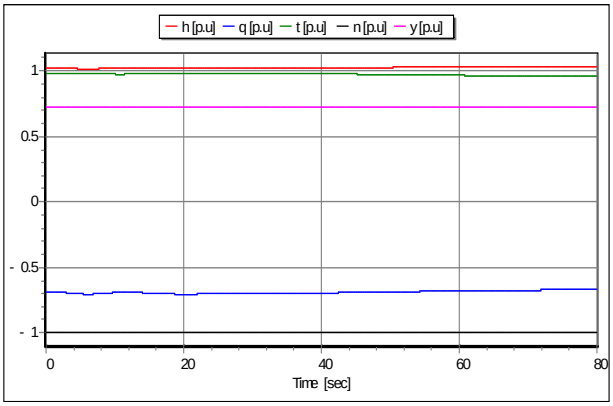

Figure 25 Transient behaviour of the pump during the decrease of irradiation.

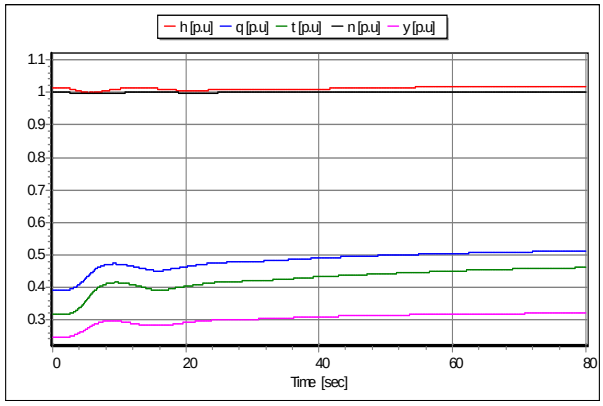

Figure 26 Transient behaviour of the turbine during the decrease of irradiation.

Via the rotational speed of the turbine, the secondary control detects that the frequency of the network is too low and hence increases its power production until the steady state error in the frequency is nil. This regulator acts on the guide vane opening of the turbine. In this case, it increases the guide vane opening to increase turbine output and hence decreasing the consumption of the hydropower plant, which is in pump mode with hydraulic short-circuit. This can be observed in Figure 24, where the power consumed by the hydropower plant slowly decreases

until 80s. The other power plants in the network, except the PV plant, have constant power production. As opposed to the case in section 8.2, the thermal power plant features almost constant power output, as the power balance is mainly achieved by the hydropower plant. Figure 25 and Figure 26 show detailed transient response of the pump and the turbine. Because the secondary control is based on the frequency deviation to increase/decrease production, it is rather slow. The frequency is fully compensated only about 80s after the beginning of the perturbation due to solar power decrease. In wide power network, measurement of frequency is the only feasible practical way to measure a power unbalance. However, in an islanded power network, where the number of power plants is small, it could be feasible to detect power unbalance by direct power measurements in the grid. Using this power measurement enables to implement more efficient secondary control in order to anticipate frequency deviations.

8.4. Sudden decrease of the sun's irradiation with secondary control based on frequency and power unbalance, case *iii)*

The initial conditions of the power flow in the islanded power network are identical to the reference case (Table 4). The same scenario as in section 8.2 is presented here, see Figure 23, except that the control of the pumped storage power plant includes secondary control that uses frequency measurement and power measurement similarly to [23]. Figure 27 shows the active power of all four power plants. As in case *ii)*, the hydropower plant is the only one, to modify its long term power production/consumption to compensate PV output changes. The hydropower plant active power setpoint is based on the on-line measurement of PV plant output.

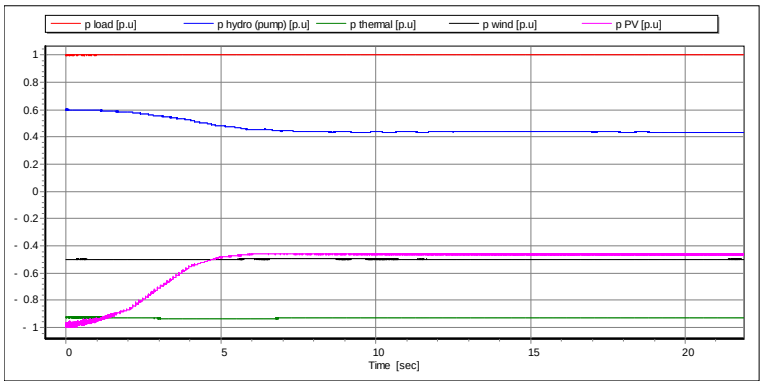

Figure 27 Active power for all 4 power plants.

As in case *ii)*, the turbine guide vanes opening increases to reduce the power consumption of the hydropower plant, which is in pump mode with hydraulic short-circuit. This can be observed in Figure 27, where the power consumed by the hydropower plant decreases within 10s. Figure 28 and Figure 29 show detailed transient response of the pump and the turbine.

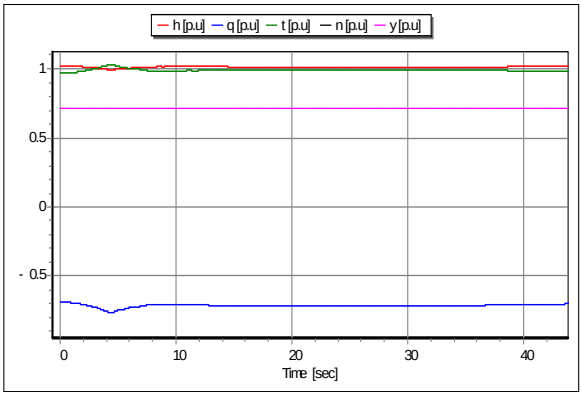

Figure 28 Transient behavior of the pump during the decrease of irradiation.

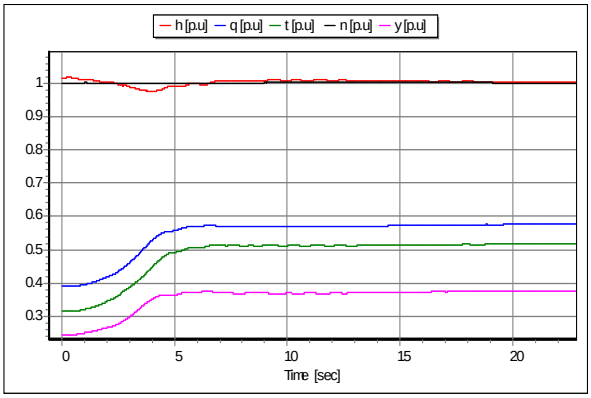

Figure 29 Transient behavior of the turbine during the decrease of irradiation.

It can be noticed that, compared to case *ii)*, the secondary control of case *iii)* reacts faster and a steady state operating of the power network is already established after 20s whereas in case *ii)* this steady state is achieved only 60 s after the perturbation. Finally, the faster response of the secondary control of case *iii)* improves the frequency stability of the network. The frequency of the network is compensated faster and magnitude of oscillations is also smaller. Figure 30 presents the comparison of the time evolution of the network frequency for

all three cases *i), ii)* and *iii)* highlighting the improvement of power network stability obtained by including secondary control at the pumped storage power plant where the frequency deviation can be reduced by factor more than 3 between cases *i)* and *iii)*.

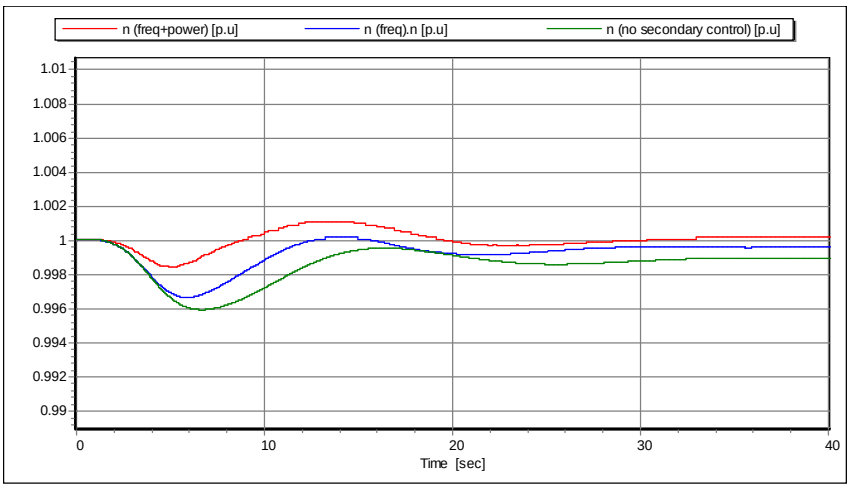

Figure 30 Comparison of power network frequency for the three scenarios *i), ii)* and *iii)* with and without secondary control.

9. Conclusions

This paper presents the modeling, simulation and analysis of a mixed islanded power network with high level of renewable energy penetration of 21% featuring 200 MW wind power plant, 100 MW PV plant, 1'300 MW thermal power plant and a 250 MW pumped storage power plant to balance the renewable production volatility. Particular attention has been paid to develop a realistic aggregated PV power plant model including an array of PV panels modeled with their UI characteristic, DC and AC filters, the DC-AC inverter modeled at the semi-conductor level, and a simplified, but realistic control based on a priori control instead of Maximum Power Point Tracking control, MPPT. This control structure enables optimal solar power conversion with reactive power set to zero. The compound ternary unit of the pumped storage power plant is operated in hydraulic short-circuit in order to provide power control in pump mode of operation when there is an excess of renewable power production. The simulation results of PV power plant sudden output power decrease, resulting from a PV cell clouds shadowing, are compared for 2 different pumped storage control strategies with the case without control. It is pointed out, that secondary control based on frequency deviation enables to compensate renewable production variations but that secondary control based on the on-line measurement of the production of the renewable energies can considerably improve the power network stability and reduce the frequency deviations by factor 3 because of the anticipation of frequency deviation.

10. Nomenclature

A: pipe cross section [m^2]
A_g: gallery cross section [m^2]
A_{ST}: surge tank cross section [m^2]
D_{ref}: machine reference diameter [m]
H: net head [m]
Q: discharge [m^3/s]
N: rotational speed [min^{-1}]
P: power [W]
T: Torque [Nm]
a: pipe wave speed [m/s]
h: piezometric head $h=z+p/(\rho g)$ [m]
g: gravity [m/s^2]
PCC: point of common connection
PV : photovoltaic
p: static pressure [Pa]
l_g: length of the gallery [m]
p: pressure [Pa]
t: time [s]
x: position [m]
y: turbine guide vane opening [-]
Z: elevation above a datum [m]
ν: specific speed
$\nu = \omega_R (Q_R / \pi)^{1/2} / (2 \cdot g \cdot H_R)^{3/4}$ [-]
ω: rotational pulsation [rd/s]
$_R$: subscript for rated

References

[1] **Akhmatov, V., Knudsen, H,** "An aggregate model of a grid-connected, large-scale, offshore wind farm for power stability investigations-importance of windmill mechanical system", Electrical power and Energy Systems 24, 2002.

[2] **Bénéteau P., Esnault F.,** "Hydrodynamique transmission de puissance cours et applications", Sciences Industrielles, ELLIPSES, 1997.

[3] **Bölcs, A.,** "Turbomachines thermiques", Vol. I, LTT/EPFL, 1993.

[4] **Bucher, R.,** "Enhanced energy balancing and grid stabilisation through 3-machine-type variable-speed pumped-storage units", Proc. Int. Conf. Hydro 2007, Granada, Spain, October 2007.

[5] **Canay, I. M.,** "Extended synchronous machine model for calculation of transient processes and stability", Electric machines and Electromechanics, vol. 1, pp. 137-150, 1977.

[6] **Delfino, F., Procopio, R., Rossi, M., Ronda, G**.,"Integration of large-size photovoltaic systems into the distribution grids: a *P-Q* chart approach to asses reactive support capability",IET Renewable Power Generation, 2010, Vol. 4, Iss 4, pp 329-340.

[7] **Godfrey, K.,** "Design and application of multifrequency signals", Computing & Control Engineering Journal, Vol. 2, Issue 4, July 1991, pp.187–195.

[8] **Heier, S.,** "Grid integration of wind energy conversion systems", Chichester : Wiley, 1998.

[9] **Jaeger, R. C.**, "Fluid transients in hydro-electric engineering practice ".Glasgow: Blackie, 1977.

[10] **Kuwabara, T., Shibuya, A., Furuta, H., Kita, E., Mitsuhashi, K.,** "Design and Dynamic Response Characteristics of 400 MW Adjustable Speed Pumped Storage Unit for Ohkawachi Power Station", IEEE Transactions on Energy Conversion, vol. 11, issue 2, pp. 376-384, June 1996.

[11] **Mohan, N., Undeland, T.M., Robbins, W. P.,** "Power Elecronics, Converters, Applications and Design", John Wiley & Sons, 2003

[12] **Nicolet, C.,** "Hydroacoustic modelling and numerical simulation of unsteady operation of hydroelectric systems", Thesis EPFL n° 3751, 2007, (http://library.epfl.ch/theses/?nr=3751).

[13] **Nicolet, C., Greiveldinger, B., Hérou, J.-J., Kawkabani, B., Allenbach, P., Simond, J.-J., Avellan, F.,** "High Order Modeling of Hydraulic Power Plant in Islanded Power Network", IEEE Transactions on Power Systems, Vol. 22, Number 4, November 2007, pp.: 1870-1881.

[14] **Nicolet, C., Vaillant, Y., Kawkabani, B., Allenbach, P., Simond, J.-J., Avellan, F.,** "Pumped Storage Units to Stabilize Mixed Islanded Power Network: a Transient Analysis", Proceedings of HYDRO 2008, October 6-9, 2008, in Ljubljana, Slovenia, Paper 16.1.

[15] **Nicolet, C., Pannatier, Y., Kawkabani, B., Schwery, A., Avellan, F., Simond, J.-J**., "Benefits of Variable Speed Pumped Storage Units in Mixed Islanded Power Network during Transient Operation", Proceedings of HYDRO 2009, in Lyon, France.

[16] **Pannatier, Y., Nicolet, C., Kawkabani, B., Simond, J.-J., Allenbach, Ph.,** "Dynamic Behavior of a 2 Variable Speed Pump-Turbine Power Plant", ICEM 2008, XVIII International Conference on Electrical Machines, Vilamoura, Portugal, September 2008.

[17] **Paynter, H. M.,** "Surge and water hammer problems". Transaction of ASCE, vol. 146, p 962-1009, 1953.

[18] **Sapin, A.,** "Logiciel modulaire pour la simulation et l'étude des systèmes d'entraînement et des réseaux électriques", Thesis EPFL n° 1346, 1995, (http://library.epfl.ch/theses/?nr=1346).

[19] **Slootweg, J. G. , De Haan, S. W. H., Polinder, H., Kling, W. L.,** "General model for representing variable speed wind turbines in power system dynamics simulations", IEEE Transactions On Power Systems, Vol. 18, No. 1, February 2003.

[20] **Slootweg J.G., Polinder H., Kling W.L.,** "Representing wind turbines electrical generating systems in fundamental frequency simulations", IEEE Transactions on energy conversion, VOL. 18, NO. 4, 2003

[21] **Souza, O.H., Jr.; Barbieri, N.; Santos, A.H.M.;** "Study of hydraulic transients in hydropower plants through simulation of nonlinear model of penstock and hydraulic turbine model," IEEE Transactions on Power Systems, vol. 14, issue 4, pp. 1269 – 1272, 1999.

[22] **Stine, W.B., Harrigan, R.W.**, "Solar Energy Systems Design", John Wiley and Sons, 1986, http://www.powerfromthesun.net

[23] **Suul, J. A., Uhlen, K., Undeland, T.,** "Variable speed pumped storage hydropopwer for integration of wind energy in isolated grids", IEEE, NORPIE/2008, Nordic Workshop on Power and Industrial Electronics, June 9-11, 2008.

[24] **Wiik, J., Gjerde, J. O., Gjengedal, T.,** "Impacts from Large Scale Integration of Wind Farms into Weak Power Systems, IEEE 2000.

[25] **Wylie, E. B. & Streeter, V.L.,** "Fluid transients in systems". Prentice Hall, Englewood Cliffs, N.J, 1993.

[26] http://www.firstsolar.com

[27] http://www.jinkosolar.com

The Authors

Christophe NICOLET graduated from the Ecole polytechnique fédérale de Lausanne, EPFL, in Switzerland, and received his Master degree in Mechanical Engineering in 2001. He obtained his PhD in 2007 from the same institution in the Laboratory for Hydraulic Machines. Since, he is managing director and principal consultant of Power Vision Engineering Sàrl in Ecublens, Switzerland. He is also lecturer at EPFL in the field of "Flow Transients in systems".

Antoine BEGUIN graduated from the Ecole polytechnique fédérale de Lausanne, EPFL, in Switzerland, and received his Master degree in Electrical Engineering in 2006. He obtained his PhD in 2011 from the same institution in the Laboratory for Power Electronics in the field of Poly-phased Matrix Converter development and optimisation. Since, he is working with Power Vision Engineering Sàrl in Ecublens, Switzerland.

Basile KAWKABANI received his master degree in 1978 from SUPELEC, Ecole Supérieure d'Electricité in Paris France, and his Ph.D. degree in 1984 from the Swiss Federal Institute of Technology in Lausanne Switzerland. He is currently a senior scientist in STI Scientists Group (Electrical Machinery). His research interests include modeling of power systems, power system stability and control.

Christian LANDRY graduated from the Ecole polytechnique fédérale de Lausanne, EPFL, in Switzerland, and received his Master degree in Mechanical Engineering in 2010. He is currently PhD student at EPFL Laboratory for Hydraulic Machines in the field of hydroacoustic modeling and hydropower plant stability analysis.

Prof. François AVELLAN graduated in Hydraulic Engineering from INPG, Ecole Nationale Supérieure d'Hydraulique, Grenoble France, in 1977 and, in 1980, got his doctoral degree in engineering from University of Aix-Marseille II, France. Research associate at EPFL in 1980, he is director of the Laboratory for Hydraulic Machines since 1994 and was appointed Ordinary Professor in 2003. Prof. F. Avellan is the Chairman of the IAHR Section on Hydraulic Machinery and Systems.